Journal of Materials Chemistry A

ROYAL SOCIETY OF CHEMISTRY

PAPER

View Article Online
View Journal | View Issue

Cite this: J. Mater. Chem. A, 2025, 13, 30480

Inverse vulcanised sulfur polymers as hydrophilic coatings

Xi Deng,* Joseph J. Dale, Pan Yang and Tom Hasell *

Sulfur polymers, synthesized by inverse vulcanisation from the industrial by-product elemental sulfur, are emerging polymeric materials with diverse applications. Incorporation of new comonomers has provided a significant boost to diversify sulfur polymer applications in recent years. However, reports on hydrophilic sulfur polymers are rare, despite the theoretical advantage of water-wetting behaviour, which enhances aqueous metal sorption by increasing the contact area. Here, we report the inverse vulcanisation of hydrophilic sulfur polymers from acids, pyrrolidone, acrylates, and amides. Structural determination of obtained sulfur polymers was investigated using nuclear magnetic resonance, and gas chromatography-mass spectrometry on the degraded polymers. The introduction of polar comonomers significantly improves polymers wettability (a minimum water contact angle of 16.4°), enabling the polymers to provide adequate contact with aqueous mercury ions. When coated onto alumina beads as adsorbents, the sulfur polymer formed from methacrylic acid (S-MAA) stands out for mercury sorption. Additionally, supporting materials were extended to silica powders, carbon black (CB) powders, and activated carbon (AC) granules for further sorption assessment. S-MAA endows the hydrophobic CB powders with hydrophilicity, showing high mercury uptake capacity (362 mg g^{-1}). Comprehensive research on hydrophilic sulfur polymers, and their applications as adsorbents, provides valuable insights for practical metal remediation.

Received 23rd April 2025
Accepted 4th August 2025

DOI: 10.1039/d5ta03218k

rsc.li/materials-a

Introduction

High sulfur-content polymers, typically synthesized through inverse vulcanisation,[1] have aroused much attention due to their potential use in metal remediation,[2] Li–S batteries,[3,4] optical materials,[5,6] antimicrobials,[7] and other fields.[8,9] Inverse vulcanisation, introduced in 2013, uses elemental sulfur (S_8) as a feedstock to react with alkenes under heat to produce sulfur polymers.[1] Initially, this process typically requires relatively high temperatures (above 159 °C) to initiate the ring-open polymerization (ROP) of S_8 into a linear polymeric sulfur with diradical chain ends, which subsequently polymerizes with vinylic comonomers to form sulfur polymers. Over the past few years, various techniques and methods (for example, catalysts,[10,11] mechanochemical synthesis,[12] photoreaction,[13] and electrochemical synthesis.[14]) have been introduced to inverse vulcanisation, resulting in reduced reaction temperatures and a wider scope of comonomers. Consequently, a variety of sulfur polymer materials have emerged. While the discovery of novel sulfur polymers matters, equally crucial is the analysis of their structures, as it provides insight into the mechanism of inverse vulcanisation which remains incompletely understood and has been described as either a radical or anionic polymerization, depending on the comonomer, catalyst, reaction conditions, and others factors involved in inverse vulcanisation.[1,10,15,16] However, detailed reports on the identification of polymer structures remain rare.[17–19] Amongst these reports, Bao *et al.* discovered the generation of linear poly(S-*r*-DIB) with bis-thiocumyl units, resulted from mono-sulfurated progress of vinyl groups.[18] In addition, Zheng *et al.* conducted small amplitude oscillation shear (SAOS) experiments to investigate the structural evolution of sulfur polymers.[17] Their findings indicate that comonomers containing alkenyl groups conjugated with aromatic rings tend to degrade into thiocarbonyls or thiophenes during polymerization. Additionally, Onose *et al.* identified the generation of aliphatic terminal structures in sulfur polymers caused by chain transfer during side reactions.[19] Confirming the structure of sulfur polymers poses challenges due to their complex polymeric units, unexpected side-reactions, and the lack of available analytical techniques; nevertheless, the process remains intriguing.

Due to the intrinsic hydrophobicity of elemental sulfur and non-polar comonomers like 1,3-diisopropenylbenzene (DIB),[18] norbornadiene,[20] plant oils,[21] limonene,[4] *etc.*, most sulfur polymers do not wet with water. In stark contrast to hydrophobic sulfur polymers, research on hydrophilic sulfur polymers is relatively uncommon.[22–28] One major challenge is the limited miscibility of molten sulfur with polar comonomers, which hinders sequent polymerization. For example,

Department of Chemistry, University of Liverpool, Liverpool L69 7ZD, UK. E-mail: xi.deng@liverpool.ac.uk; t.hasell@liverpool.ac.uk

polymerization may occur at the phase interface, greatly extending reaction time or leading to incomplete reaction, producing a heterogenous product. However, hydrophilic sulfur polymers could be advantageous, particularly in the context of mercury capture in wastewater. The conventional strategy for improving mercury sorption involves increasing the contact sites for mercury ions onto sulfur polymers, specifically by rendering the polymers as coatings,[29] fibers,[30] foams,[22] particles,[31] and porous structures.[32] Recently, hydrophilic and water-soluble sulfur polymers have emerged as a promising approach for mercury capture. Limjuco *et al.* synthesized hydrophilic sulfur polymers from 2-carboxyethyl acrylate (CEA), which showed high Hg^{2+} capture efficiency as microfibrous composites.[25] Moreover, Eder *et al.* reported charged sulfur polymers that readily dissolve in water and bind with aqueous metal ions, acting as flocculants.[24]

Herein, we report the synthesis of a series of hydrophilic sulfur polymers with water contact angles as low as 16.4°, demonstrating significantly enhanced water wetting behaviour, approximately a sevenfold reduction in contact angle, compared to conventional hydrophobic sulfur polymers (112.2° when synthesized with sunflower oil).[23] In addition, detailed structural analysis was conducted for each polymer, identifying both doubly (crosslinked or linear) and mono-sulfurated (terminal) polymers in final products. The hydrophilicity endows sulfur polymers with adequate contact sites for mercury ions as coatings on Al_2O_3 beads. Amongst these samples, sulfur polymer S-MAA from methacrylic acid showed superior performance on mercury sorption and was selected as the model coating material. Moreover, various supporting materials such as silica powders, carbon black (CB) powders, and activated carbon (AC) granules, were explored and evaluated for mercury sorption. Notably, S-MAA coated CB powders (S-MAA@CB) achieved a high effective mercury sorption (above 99%) under both neutral and acid conditions. In this work, the use of commercially available comonomers acrylic acid (AA) and *N*-vinylpyrrolidone (NVP) is reported in inverse vulcanisation for the first time. In addition, the detailed synthesis and characterization of other rarely reported sulfur polymers are also thoroughly investigated. Considering that there is a large surplus in the production of sulfur, and there is hope that industrial polymers may be developed using at least part of this surplus, there is in polymer chemistry a continuous search for methods to synthesise polymers of sulfur that could find novel applications.[33] The use of such highly industrially available common monomers such as those reported here is therefore advantageous.

Results and discussion

Synthesis and characterizations of sulfur polymers

As illustrated in Scheme 1, eight sulfur polymers were synthesized using elemental sulfur (S_8) and comonomers acrylic acid (AA), methacrylic acid (MAA), *N*-vinylpyrrolidone (NVP), 2-hydroxyethyl acrylate (HEA), hydroxyethyl methacrylate (HEMA), acrylamide (AAm), poly(ethylene glycol) diacrylate (PEGDA250), and ethylene glycol dimethylacrylate (EGDMA)

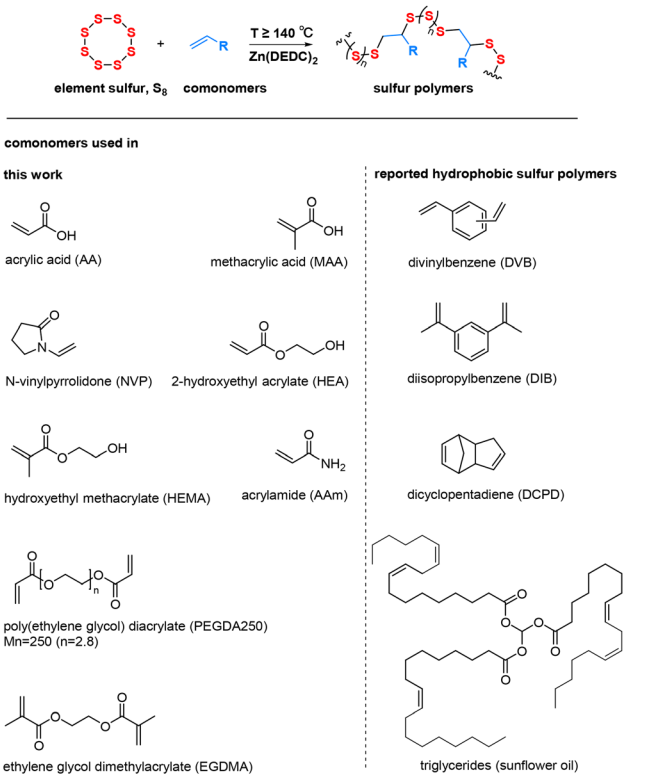

Scheme 1 General reaction of elemental sulfur and comonomers. The top panel shows the synthesis of inversed vulcanised sulfur polymers. The bottom panel shows the comonomers used in this work as well as those in other reported conventional hydrophobic sulfur polymers.

(S_8 : comonomers = 1 : 1 in mass ratio). The resulting polymers were named S-AA, S-MAA, S-NVP, S-HEA, S-HEMA, S-AAm, S-PEGDA250 and S-EGDMA (photographs are shown in Fig. 1a). S-AA and S-MAA were synthesized under reflux for 24 h to prevent the evaporation of the comonomers, as the reaction temperatures (140 °C for S-AA and 160 °C for S-MAA) are close to the boiling points of the comonomers (Table S1). Attempts to synthesize S-AA and S-MAA at lower temperature (135 °C for S-AA, and 135, 150 °C for S-MAA) showed negligible polymerization, where obvious phase separation occurred (Fig. S1). The remaining polymers were synthesized following the general inverse vulcanisation methods under different synthesis conditions (Table S2). Catalyst zinc diethyldithiocarbamate $Zn(DEDC)_2$ was used in this work to enhance reactivity of sulfur and comonomers, as has been evidenced by Wu *et al.* and Dodd *et al.*[10,11] For example, compared to the non-catalytic reaction, $Zn(DEDC)_2$ promoted the complete consumption of C=C bonds in MAA during S-MAA synthesis (Fig. S2). The addition of $Zn(DEDC)_2$ to the mixture of sulfur and AAm caused severe auto-acceleration, likely due to the self-activation of AAm.[34,35] Therefore, no catalyst was added in the synthesis of S-AAm.

Nuclear magnetic resonance (NMR) analysis of sulfur polymers is often challenging due to their insolubility and the complex microstructural mixtures resulting from side reactions during inverse vulcanisation; therefore, detailed structures and by-products of sulfur polymers are not always fully

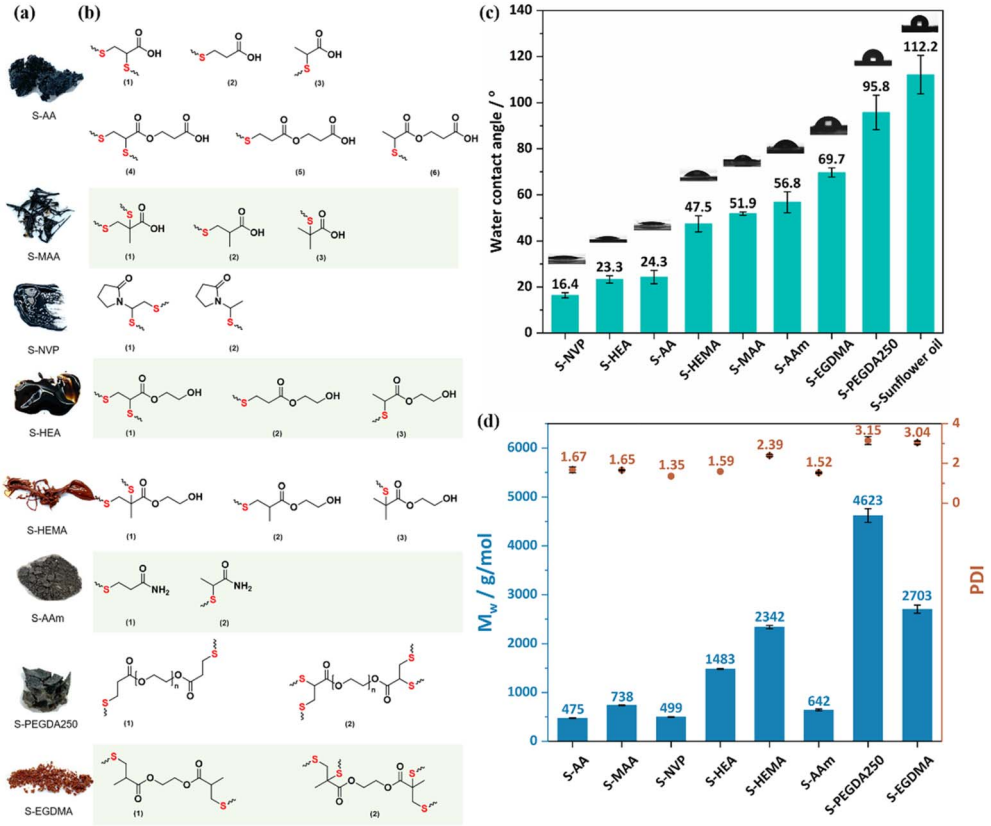

Fig. 1 (a) Photographs of S-AA (black tacky solid), S-MAA (black viscous liquid), S-NVP (dark brown viscous liquid), S-HEA (dark brown viscous liquid), S-HEMA (reddish-brown viscous liquid), S-AAm (black brittle solid), S-PEGDA250 (brown elastic solid), S-EGDMA (reddish-brown brittle solid). (b) The middle panel displays the proposed structural components of each polymer. (c) The water contact angle (WCA) of sulfur polymers. (d) The molecular weight and dispersity index of sulfur polymers tested by GPC. Of note, GPC test was conducted using the soluble portion of polymers in tetrahydrofuran (THF) with a concentration of 3 mg mL^{-1}.

recognized.[18,19,36] In this work, S-AA, S-MAA, S-NVP, S-HEA, S-HEMA readily dissolved in deuterated dimethylsulfoxide ($DMSO\text{-}d_6$) or chloroform ($CDCl_3$), whereas S-AAm, S-PEGDA250 and S-EGDMA partially do. This enabled further elucidation of the polymeric structures. The obtained sulfur polymers were subject to solution ^1H, ^{13}C NMR (Fig. S3–S10). The reaction of comonomers after inverse vulcanisation was confirmed by the disappearance of signals related to C=C bonds. Notably, trace proton peaks (7.0–9.5 ppm) attributed to aldehydes were observed in polymers, except for S-AAm, likely resulting from the addition of peroxyl radicals generated by oxygen onto the comonomers, as the reaction occurred in an open air condition.[37,38] The original inverse vulcanisation mechanism, as proposed in 2013 for crosslinked poly(S-*r*-DIB), suggests that double sulfuration occurs at each isopropenyl group in 1,3-diisopropenylbenzene (DIB), forming two C–S bonds.[1] Recently, the discovery of linear poly(S-*r*-DIB) with bis-thiocumyl has highlighted a new mechanism of inverse vulcanisation.[18] This newly proposed mechanism suggests the formation of a single C–S bond through mono-sulfuration of the isopropenyl group in DIB, along with the generation of thio-cumyl groups through hydrogen abstraction. Hence, doubly (crosslinked or linear) and mono-sulfurated (terminal) structures in sulfur polymers must be considered. The detailed structural analysis of obtained sulfur polymers was conducted by distortionless enhancement by polarization transfer (DEPT) 135 and heteronuclear single quantum coherence (HSQC) NMR (Fig. S11–S21). All the assumed structures of each sulfur polymer are summarized in Fig. 1b. For polymer S-AA, two unexpected methylene signals (C_g, 61 ppm and C_c, 34 ppm) were detected, likely assigned to α- and β-CH_2 in the form of $–COOCH_2CH_2–$ segments (Fig. S11). A hypothesis is that conjugate addition occurred, leading to the formation of 2-carboxyethyl acrylate (CEA) from AA during inverse vulcanisation. In a control experiment where AA was heated to equivalent conditions without sulfur, similar methylene peaks at 60 and 34 ppm as well (Fig. S12) were observed, supporting the hypothesis. The conjugate addition mechanism was assumed in Fig. S13. AA tautomerized to form electrophilic enolates. In addition, AA was deprotonated to generate carboxylate nucleophiles $–COO^-$, which reacted with the enolate in a conjugate addition reaction. Finally, the resulting enolate intermediate abstracted protons to form the dimers CEA.[39] Consequently, both AA and CEA were involved as comonomers in the polymerization with sulfur. As shown in Fig. S11, carbon resonances observed in S-AA correspond to methyl (C_a, 12 ppm) and methine (C_e, 41 ppm) from terminal

structures 3 and 6. In addition, terminal polymers 2 and 5 were verified by two signals of secondary carbons (C_b, 27 ppm and C_d, 34–35 ppm). The downfield secondary carbons (C_f, 42 ppm) can be rationalized by the linear polymer 1 and 4. In conclusion, polymer S-AA comprises linear and terminal units derived from AA and CEA. For polymer S-MAA, no conjugate addition was observed despite the structural similarity between MAA and AA (Fig. S14). A doubly sulfurated linear structure 1 and two mono-sulfurated terminal structures 2 and 3 in S-MAA were detected. In polymer 1, secondary carbons (C_e, 48, 50 ppm) were detected, and shifted further downfield due to the presence of two adjacent sulfur atoms, in contrast to the mono-sulfur adjacent carbons (C_d, 42 ppm) in structure 2. Tertiary carbons (C_c, 39 ppm) are also the evidence for structure 2. Furthermore, a new signal for primary carbons (C_b, 24–28 ppm), not MAA's own methyl carbons (C_a, 17 ppm), belongs to polymer 3 with a thio-isopropyl group. Moreover, quaternary carbons (C_f, 55–57 ppm) in structure 1 and 3 were not evident in the DEPT 135 spectrum. In the case of polymer S-NVP, two structures were identified: a linear structure 1 and a terminal structure 2 (Fig. S15). This was supported by signals of secondary carbons (C_e, 46–50 ppm) and tertiary carbons (C_f, 58 ppm) in polymer 1, as well as primary C_a (18 ppm) in polymer 2. The absence of other secondary carbon signals ruled out the possibility of a terminal structure containing a β-thio-ethyl group. With respect to polymer S-HEA, three signals attributed to secondary carbons were discovered (C_b, 27 ppm; C_c, 34 ppm; C_e, 47–49 ppm) (Fig. S16). These signals indicate the presence of linear polymer 1 and terminal polymer 2. Meanwhile, a signal at 11–13 ppm was observed, assigned to the methyl carbon C_a in terminal polymer 3. Regarding polymer S-HEMA, a linear and two terminal species were proposed (Fig. S17). Two signals originating from secondary carbons at 43 ppm (C_d) and 39 ppm (C_c) were assigned to polymer 1 and 2, respectively. Polymer 3, featuring a thio-isopropyl group, was confirmed by the absence of quaternary carbons (C_h, 46, 48 ppm) and the appearance of new primary carbons (C_b, 25 ppm) in DEPT 135 spectrum. Polymers S-PEGDA250 and S-EGDMA partially dissolve in NMR solvents, theoretically due to the presence of an insoluble crosslinked portion. However, poor solubility of S-AAm was also observed. In a control experiment, AAm was heated under equivalent conditions without sulfur, but the product's solubility in DMSO was also inadequate for NMR analysis. The following hypotheses may explain this anomalous phenomenon: (i) AAm may undergo imidization upon heating above 100 °C, leading to crosslinking with sulfur (the assumed intermolecular imidization was illustrated Fig. S18).[40] (ii) Intermolecular hydrogen bonds may create stable polymeric networks that hinder the entry of S-AAm into solvents.[41] Due to the partial dissolution of S-AAm, S-PEGDA250, and S-EGDMA in NMR solvents, the proposed structural analysis is limited to the soluble section of each polymer. For polymer S-AAm, two mono-sulfurated terminal species were suggested (Fig. S19). Species 1 shows two signals from methylene carbons (C_c, 36 ppm and C_b, 27 ppm), indicating a β-thio-ethyl group. Species 2 exhibits signals for methyl carbons (C_a, 19 ppm) and tertiary carbons (C_d, 42 ppm), indicative of the α-thio-ethyl group. In S-PEGDA250, a linear structure 1 was proposed, as evidenced by two secondary carbons (C_a, 27 ppm and C_b, 34 ppm), with no tertiary and primary carbon signals (Fig. S20). Similarly, a linear structure 1 was found in polymer S-EGDMA according to new signals of tertiary carbons (C_b, 24 ppm) and secondary carbons (C_c, 43 ppm) next to sulfur atoms (Fig. S21).

Recently, the degradation of sulfur polymers using lithium aluminium hydride ($LiAlH_4$), which cleaves S–S bonds and generates thiols with monomeric units, has been applied to further structural confirmation.[14,20,42] These resulting thiols are either purified by silica gel chromatography for solution NMR analysis, or analysed directly using gas chromatography-mass spectrometry (GC-MS). In this work, sulfur polymers were treated with $LiAlH_4$, and the resulting product mixtures were analysed by NMR and GC-MS. The detailed structural analysis was concluded in Fig. S22–S37. Complete reduction of carboxyl acids and esters to alcohols, and amides to amines in sulfur polymers was confirmed by the loss of the carbonyl carbon signal in NMR spectra.[43] However, incomplete cleavage of S–S bonds resulted in less broad peaks, compared to those of the pristine polymers. Moreover, GC-MS analysis revealed the presence of thiols, consistent with the assumed thiols derived from previously proposed polymer structures (excluding S-NVP and S-AAm). The peak signals of degraded S-NVP and S-AAm are quite weak and do not align with any of the proposed thiol structures. These findings indicate that, despite sulfur polymers with easily reducible functional groups did not readily undergo complete degradation, valuable structural information was still collected which aided polymer structure elucidation.

The successful synthesis of sulfur polymers was further evidenced by Fourier-transform infrared (FTIR) spectra (Fig. S38–S45). The alkene C=C stretching vibrations at 1610–1637 cm^{-1} in comonomers disappeared or significantly weakened after inverse vulcanisation. In addition, characteristic peaks induced by C=O bonds (1667–1728 cm^{-1}) were observed in all samples, along with C–O bonds (1149–1238 cm^{-1}) in polymers containing ester groups, and C–N bonds in S-NVP (1408 cm^{-1}) and in S-AAm (1394 cm^{-1}). It is reported that primary amine groups in oleylamine likely participate in inverse vulcanisation, forming secondary amines, as evidenced by a noticeable shift of N–H bonds to a lower wavenumber in FTIR.[44] However, in S-AAm, no significant N–H bonds shift was observed, indicating no reaction between NH_2 in amides and sulfur. This is probably because the nucleophilicity of the amine long pair is reduced by conjugation into the amide oxygen. CHNS elemental analysis is presented in Table S3. Sulfur polymers, except S-AAm, with predetermined 50 wt% sulfur have roughly equivalent composition of elements to the theoretical values. In terms of S-AAm, two measurements showed a significant difference in carbon and sulfur content, indicative of the heterogeneity of the polymer. The thermal properties of the polymers were characterized by thermogravimetric analysis (TGA) and differential scanning calorimetry (DSC). TGA illustrates that $T_{deg,\ 5\%}$ of sulfur polymers ranges from 138 to 215 °C (Fig. S46). Glass transition temperatures (T_g) were recorded as: −28.9 °C (S-AA), −19.0 °C (S-MAA), −30.4 °C (S-NVP), −36.1 °C (S-HEA), −15.6 °C (S-HEMA), 70.0 °C (S-AAm), −25.4 °C (S-PEGDA250), and 15.1 °C

(S-EGDMA) (Fig. S47). Distinct crystal sulfur peaks at ≈105 and 116 °C were discovered in DSC curves for S-AA, S-AAm and S-PEGDA250, due to the unreacted sulfur. Traces of crystal and amorphous sulfur were identified in all polymers, proved by powder X-ray diffraction PXRD and thin layer chromatography TLC (Fig. S48 and S49).

Common sulfur polymers using divinylbenzene (DVB), 1,3-diisopropenylbenzene (DIB), and dicyclopentadiene (DCPD) as comonomers exhibited limited hydrophilicity, with water contact angle (WCA) exceeding 83.5°.[23] Notably, polymeric sulfur–sunflower oil demonstrates high hydrophobicity with a WCA of 112.2°. However, in this work, the incorporation of hydrophilic comonomers enhanced the wettability of sulfur polymers. As shown in Fig. 1c, S-NVP is the most hydrophilic (with a lowest WCA of 16.4°), followed by S-HEA (23.3°), S-AA (24.3°), S-HEMA (47.5°), S-MAA (51.9°), and S-AAm (56.8°). In contrast, S-EGDMA is less hydrophilic (69.7°), while S-PEGDA250 is hydrophobic (95.8°). This is because comonomers EGDMA and PEGDA250 bearing hydroneutral ester groups show minimal impact on improving the wettability of sulfur polymers.[45] Solubility tests of sulfur polymers in water and common organic solvents were carried out (Fig. S50 and S51). S-AA, S-NVP, S-HEA, and S-AAm slightly dissolved in water with soluble fractions of 22.02, 12.67, 10.68, and 16.31%, respectively. The remaining polymers are water-insoluble. Regarding these four polymers, the soluble and insoluble fractions were collected and analysed by CHNS (Table S4). The higher C/S ratio in the soluble portion than the insoluble portion indicates a difference in chemical composition. This suggests that the soluble portion consists of small thiols isolated from the polymeric backbone. To ensure that the limited water solubility of these four polymers was not due to solution saturation, which hindered further dissolution of the polymer, repeated dissolution tests were carried out on the insoluble fraction. After three repetitions, the soluble fractions all dropped to below 3.40% (Table S5), confirming minimal dissolution. Therefore, in contrast to previously reported charged sulfur polymers that readily dissolve in water, the hydrophilic sulfur polymers in this work, which bear electroneutral units, exhibit poor water solubility.[23,24] Gel permeation chromatography (GPC) analysis illustrates that the obtained sulfur polymers are oligomers with diverse molecular weights M_w: 475 g mol^{-1} (S-AA), 738 g mol^{-1} (S-MAA), 499 g mol^{-1} (S-NVP), 1483 g mol^{-1} (S-HEA), 2342 g mol^{-1} (S-HEMA), 642 g mol^{-1} (S-AAm), 4623 g mol^{-1} (S-PEGDA250), and 2703 g mol^{-1} (S-EGDMA) (Fig. 1d). The low molecular weight of polymers likely resulted from the linear and terminal structures, as previously proposed in NMR section.

Fabrication and mercury capture of sulfur polymer-coated alumina (SP@Al_2O_3) beads

Given that the synthesized polymers are sticky and bulky, providing limited availability of Hg^{2+} binding sites, their direct application for mercury capture in aqueous solutions may be awkward. Therefore, grafting of sulfur polymers onto supporting materials (*e.g.* alumina Al_2O_3 beads) could address this issue.

A soaking method was applied and briefly described here (see the SI for details), which involved preparing polymer-in-THF solutions, soaking Al_2O_3 beads in the solution, then isolating, washing, and drying the beads to obtain the sulfur polymer coated beads SP@Al_2O_3 (Fig. 2a). This method allows the polymers-in-THF solution to be reused, enabling scale-up in real systems. Upon coating, the original white beads turned to brown or yellow (Fig. 2b and S52). Taking S-MAA@Al_2O_3 beads as an example, energy-dispersive X-ray (EDX) analysis confirms the presence of sulfur from the polymer; however, scanning electron microscope (SEM) reveals that the coating was not ideally uniform, as evidenced by the uncoated dark areas (Fig. 2c). No significant polymer signals were detected in coated beads by FTIR (Fig. S53). The coating ratio for each bead, calculated based on the mass loss of polymers measured by TGA, ranges from 1.86 to 7.90% (polymers/uncoated beads, wt%) (Fig. S54). Pristine Al_2O_3 beads exhibit a Brunauer–Emmett–Teller (BET) surface area of 209 m^2 g^{-1}, which decreased to 79–190 m^2 g^{-1} after polymer coating (Fig. S55). To a certain extent, sulfur polymers occupied the pore sites of the beads (Table S6).

Sulfur polymer coated porous supports exhibit potential as mercury sorbents in water, with three key attributes in this regard: amount of coated sulfur polymers, surface area, and hydrophilicity. To evaluate the influence of these attributes on the mercury adsorption, mercury capture was conducted using SP@Al_2O_3 beads. 50 mg of SP@Al_2O_3 beads were applied to 10 mL of $HgCl_2$ aqueous solutions (500 ppm). Fig. 2d–f present the Hg^{2+} uptake capacity of the beads as a function of coating ratio, BET surface area, and polymer wettability. Uncoated Al_2O_3 beads were initially chosen to test due to their high surface area and moderate binding affinity for Hg^{2+} on their own.[46] In addition, the relatively large size Al_2O_3 beads make them convenient for handing and separation. However, after coating, some SP@Al_2O_3 beads exhibited lower capacities than uncoated Al_2O_3 beads, which is likely from the relative affinity for Hg^{2+} of Al_2O_3/polymers, as well as the blocking of pores. As well as mercury being captured from solution into the solid phase, there is the potential for undesirable leaching of partially soluble polymers or sulfur into the aqueous phase. Notably, when used as coatings, the leaching of sulfur polymers into the aqueous solution can be mitigated, thereby reducing secondary contamination to some extent. For example, using S-AA as a coating reduced its leaching by approximately sixfold (Fig. S56). Amongst these beads, S-MAA@Al_2O_3 beads demonstrated a binding efficiency of 28.96% and a capacity of 33 mg g^{-1} for Hg^{2+}, which outperformed the other beads (Table S7). However, S-MAA@Al_2O_3 beads showed no significant advantages in coating ratio, BET surface area, or hydrophilicity compared to other SP@Al_2O_3 beads. This indicates ranking these three factors in terms of their importance for mercury adsorption is complex, and likely involves trade-offs. Overall, sulfur polymer S-MAA stood out from other polymers in mercury uptake performance, and thus was selected as the model coating for subsequent mercury uptake tests.

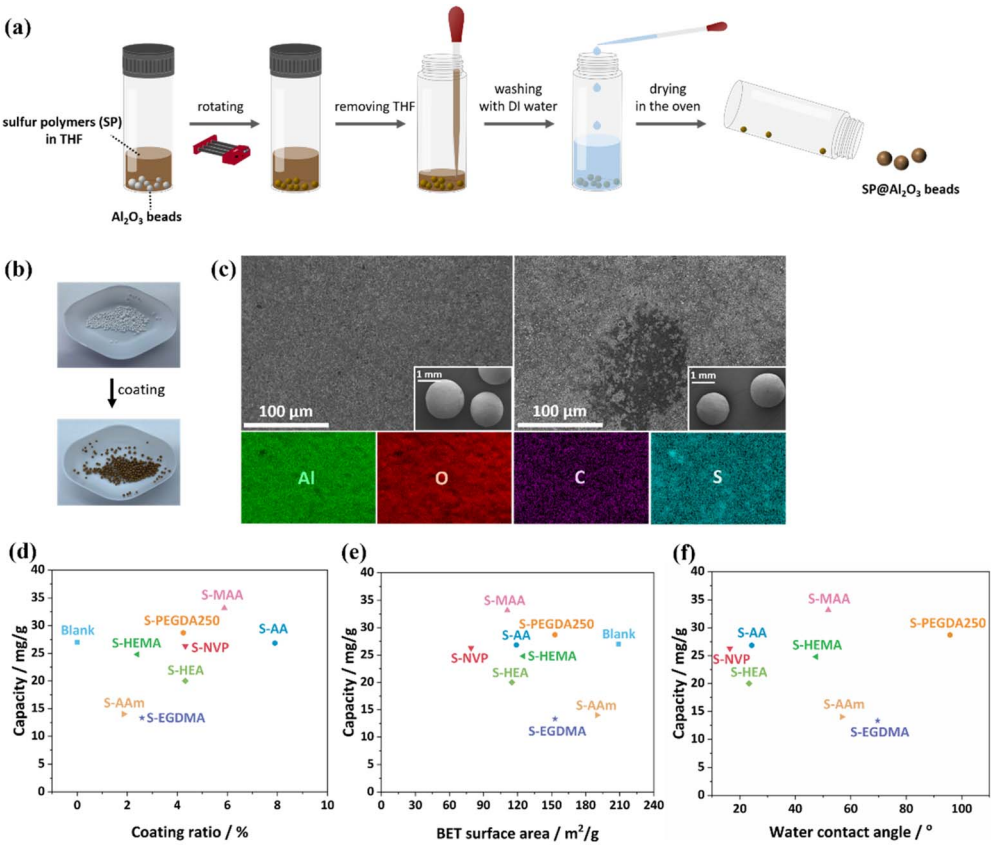

Fig. 2 (a) Schematic illustration for the preparation of SP@Al_2O_3 beads. (b) Photographs of uncoated and S-MAA@Al_2O_3 beads. (c) Scanning electron microscope (SEM) images of uncoated (left) and S-MAA@Al_2O_3 (right) beads. The inset is the magnified view. The below is energy-dispersive X-ray (EDX) maps of S-MAA@Al_2O_3 beads. Relationships between mercury uptake capacity and (d) coating ratio, (e) BET surface area of SP@Al_2O_3 beads and (f) water contact angles of sulfur polymers. Of note, 'g' in the capacity unit 'mg g^{-1}' refers to the mass of the coated beads, not the polymers.

Comparison of different S-MAA-coated composites

Silica (SiO_2) powders, carbon black (CB) powders, and activated carbon (AC) granules were also used as substrates and coated with S-MAA, following the soaking method to produce S-MAA@SiO_2 powders, S-MAA@CB powders, and S-MAA@AC granules. The presence of hydrogen bonds was inferred to strengthen the interactions between S-MAA and both Al_2O_3 beads and SiO_2 powders. Additionally, CB was proved to efficiently trap sulfur radicals, thereby promoting the grafting of sulfur polymers.[8] The interaction between S-MAA and activated carbon remains obscure. Four S-MAA/inorganic composites are visualized in Fig. S57. As shown in SEM and EDX images (Fig. 2c and S58–S60), S-MAA@Al_2O_3 beads are spherical, with an average diameter of 1 mm. S-MAA@SiO_2 powders are irregular, averaging 50 μm in size. Clusters of S-MAA@CB powders exhibit a wide range of sizes at the micron scale. The pore structure of millimetre-sized S-MAA@AC granules was also witnessed. Successful grafting of polymer S-MAA onto the substrates was evidenced by EDX, where elemental sulfur was detected. In addition, the decrease in BET surface area is indicative of polymer loading onto the substrates: from 209 $m^2\ g^{-1}$ to 111 $m^2\ g^{-1}$ (S-MAA@Al_2O_3 beads), from 365 $m^2\ g^{-1}$ to 323 $m^2\ g^{-1}$ (S-MAA@SiO_2 powders), from 28 $m^2\ g^{-1}$ to undetectable (S-MAA@CB powders), and from 584 $m^2\ g^{-1}$ to 283 $m^2\ g^{-1}$ (S-MAA@AC granules) (Fig. S61). Mercury uptake tests were conducted to evaluate the performance of S-MAA coated materials, with the removal of Hg^{2+} at 500 ppm shown in Fig. 3a. The S-MAA itself, without carrier materials, has an Hg^{2+} capacity of 28 mg g^{-1} and removal efficiency of 27.68%. This adsorption performance is not particularly impressive, and a key reason is the limited contact between the bulk polymer and the ions. For Al_2O_3 beads, the incorporation of sulfur polymers resulted in a slight uplift by 5.38% in removal efficiency. In contrast, S-MAA@SiO_2 powders exhibited 23.09% removal of mercury, whereas the uncoated powders showed negligible Hg^{2+} adsorption. An uptake efficiency of 99.05% endowed S-MAA@CB powders with considerable potential as mercury adsorbents. The high efficiency is likely due to the substantial sulfur polymer loading onto CB powders (coating ratio of 57.08%), which enhanced Hg^{2+} capture despite the powders' limited surface area. However, a decline in uptake was observed in the case of S-MAA@AC granules, which possibly resulted from a reduction in surface area, leading to the loss of available binding sites. Sorption isotherms for coated and uncoated AC granules were depicted to investigate performance at low concentration (Fig. S62). Uncoated AC granules exhibited a sharp uptake, while S-MAA@AC granules showed a moderate

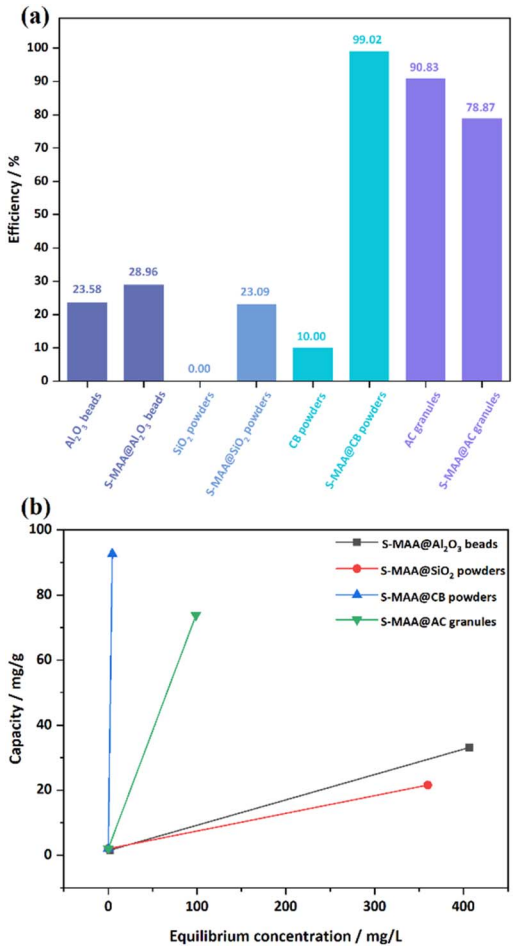

Fig. 3 (a) Comparison of Hg^{2+} (500 ppm) capture using uncoated supports, and the corresponding S-MAA coated composites. (b) Simplified isotherm of Hg^{2+} (10 ppm and 500 ppm) adsorption onto four composites. The steep line demonstrates the sharp mercury uptake.

sorption. The coating of S-MAA onto AC granules appears to be less effective for mercury capture. S-MAA@Al_2O_3 beads, S-MAA@SiO_2 powders, S-MAA@CB powders, and S-MAA@AC granules presented capacities of 33, 22, 93, and 74 mg g^{-1}, respectively at a Hg^{2+} concentration of 500 ppm. The capacity was calculated based on composites mass. The capacity calculation based on polymer mass is displayed in Fig. S63.

In practical scenarios, mercury adsorbents are unlikely to encounter wastewater with large concentrations of mercury. Therefore, the ability to treat low concentration wastewater is an important consideration for adsorbents. As long as the adsorbents demonstrate sharp uptake at low concentrations, they can be used effectively. Removal of 10 ppm Hg^{2+} was also tested. S-MAA@SiO_2 powders, S-MAA@CB powders, and S-MAA@AC granules achieved removals up to 99.22, 99.56, and 99.67%, respectively, while S-MAA@Al_2O_3 beads showed an adequate uptake of 79.25%. Results from low (10 ppm) and high (500 ppm) concentration experimental groups are summarised in Fig. 3b. The simplified isotherm represents a rough comparison of the adsorption ability of each composite, noting that the steeper the line the more effective the adsorbent is. Among these composites, S-MAA@CB powders performed the best and were further applied in mercury capture tests.

Mercury capture of S-MAA@CB powders

As shown in Fig. 4a and b, the untreated CB powders are hydrophobic, with a WCA of 139.09°, and they float on the water's surface rather than entering water. This floating behaviour weakens their contact with mercury ions in aqueous solutions. Similarly, when hydrophobic S–sunflower oil was used as a coating, the obtained powders also floated on the water surface, resulting in poor Hg^{2+} adsorption performance, with an uptake efficiency of only 5.06% and a capacity of 5 mg g^{-1}. However, upon coating with S-MAA, CB powders became hydrophilic and could be wetted and well dispersed in water. The marked change in wettability has endowed CB powders with new potential as adsorbents, and it increases the likelihood of binding with mercury ions.

The maximum mercury sorption capacity is a key parameter in evaluating adsorbents. However, in practical scenarios, absorbents are unlikely to encounter the amounts and concentrations of Hg^{2+} necessary to achieve saturation capacities. As long as materials with an appreciable capacity (*e.g.* over 100 mg g^{-1}) ideally exhibit a steep uptake at low concentration, they can be used effectively. Fig. 4c reveals high affinity of S-MAA@CB powders for Hg^{2+}, fitted well with Langmuir model (R^2 = 0.9197). The saturation capacity was found to be 362 mg g^{-1}, which is comparable to that of reported hydrophobic mercury adsorbents, and is more than adequate for practical use (Table S8). S-MAA@CB powders nearly removed all mercury at low concentration; for example, reducing Hg^{2+} from 250 ppm to 2.4 ppm. The sharp initial uptake at low concentrations highlights the material a favourable adsorbent.

In real life, mercury pollution exists in household water and the ocean, where sodium chloride is common and found to interfere with mercury sorption by reducing the rate and amount of mercury capture.[47] Accordingly, Hg^{2+} uptake (500 ppm) by S-MAA@CB powders was analysed kinetically in DI water, simulated tap water (6.85 mM NaCl) and seawater (599 mM NaCl) (Fig. 4d). After 24 hours, S-MAA@CB powders exhibited Hg^{2+} uptakes of 270 mg g^{-1} (DI water) and 261 mg g^{-1} (tap water), corresponding to 66.40% and 64.15% removal. This similarity suggests that low NaCl levels do not significantly affect mercury sorption. However, a dramatic reduction in uptake (76 mg g^{-1}) and removal (18.59%) was observed in simulated seawater, indicating that high NaCl levels hinder the adsorption performance of S-MAA@CB powders, likely due to competition between NaCl and Hg^{2+} for binding sites on the composite.

The Hg^{2+} removal process may be affected by solution pH; therefore, mercury solutions with various pH were applied to assess the sorption performance of S-MAA@CB powders. As shown in Fig. 4e, S-MAA@CB powders achieved a 99.37% removal of Hg^{2+} in a neutral solution. At pH 4, the acidity had negligible effect on mercury sorption, with removal remaining at 99.29%. Due to the presence of –COOH groups in S-MAA, no

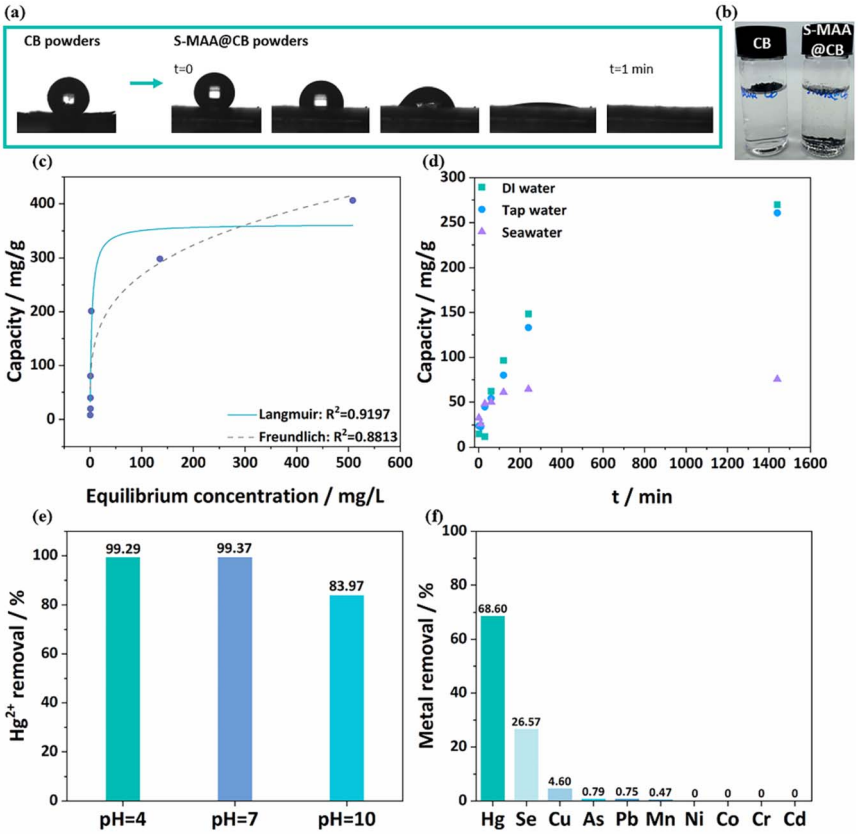

Fig. 4 (a) Photographs of wettability tests on uncoated and S-MAA@CB powders. Hydrophobic CB powders exhibited a WCA of 139.09°. The hydrophilicity of S-MAA@CB powders was proved by their rapid water wetting behaviour within one minute. (b) Photographs of uncoated CB (left) and S-MAA@CB (right) powders disperse in water. (c) Isotherm of Hg^{2+} (10, 25, 50, 100, 250, 500, and 1000 ppm) onto S-MAA@CB powders, fitted to Langmuir and Freundlich models, respectively. (d) Kinetics of Hg^{2+} (500 ppm) onto S-MAA@CB powders in DI water, simulated tap water and seawater. (e) Effect of pH on Hg^{2+} (100 ppm) onto S-MAA@CB powders. (f) Selectivity of S-MAA@CB powders using a mixed metal ion solution.

protonation occurred to repel Hg^{2+} binding on S-MAA through electrostatic barriers under acidic conditions.[48] Nevertheless, sorption in the alkaline solution (pH 10) resulted in the attenuation of mercury removal (83.97%), likely due to the precipitation of hydroxide species $Hg(OH)^+$ and $Hg(OH)_2$ on the material surface, which blocks active sites and reduces retention.[49] Additionally, hydroxide might break S–S bonds in the polymer, hindering the sorption.[47]

Although the high mercury capture capacity of S-MAA@CB powders is noteworthy, their performance was also evaluated under more practical conditions, specifically at low mercury concentrations with competing metal ions. A trace metals solution (certified reference material, CRM) with ion concentrations at ppb levels was applied to simulate real industrial wastewater. As depicted in Fig. 4f and Table S9, S-MAA@CB powders captured 68.60% of Hg^{2+} in one hour, with concentration decreasing to 1.313 ppb. Moreover, 26.57% of selenium (Se) ions were adsorbed, while other ions were largely unaffected. S-MAA@CB powders demonstrated high selectivity for Hg^{2+}, as competing ions at low concentrations did not affect the sorption. Meanwhile, S-MAA@CB powders demonstrated a potential for Au^{3+} adsorption, effectively reducing the concentration of Au^{3+} from 500 ppm to 0.7 ppm, corresponding to an efficiency of 99.8%.

S-MAA@CB powders, after binding mercury in 1000 ppm Hg^{2+} test, were collected as S-MAA@CB/Hg, and their composition was analysed *via* X-ray photoelectron spectroscopy (XPS) (Fig. 5). New peaks corresponding to Hg 4p, 4d, 4f, and 5d confirmed Hg^{2+} accumulation onto the composite surface. To investigate Hg^{2+} interactions with the powders, high-resolution S 2p spectrum in S-MAA@CB revealed peaks related to C–S (162.0 and 163.1 eV) and S–S (163.8 and 165.0 eV) bonds. After sorption, C–S bonds displayed higher binding energy, implying the generation of coordinate bonds as C–S–Hg^{2+}.[48] However, no significant shift occurred regarding S–S bonds, indicative of no detectable coordination between S–S bonds and Hg^{2+}. Further, O 1s spectrum was studied due to oxygen's potential as a Hg^{2+} binding site, yet no significant interaction with mercury was observed (Fig. S64a). PXRD analysis (Fig. S64b) reveals no characteristic peaks for hexagonal (wurtzite) α-HgS or cubic (zinc blende) β-HgS, indicative of no generation of crystalline HgS after sorption.[50] The lack of detected crystallinity is consistent with the Hg^{2+} being bound by the sulfur polymer, rather than crystallising with free sulfur. SEM imaging shows no

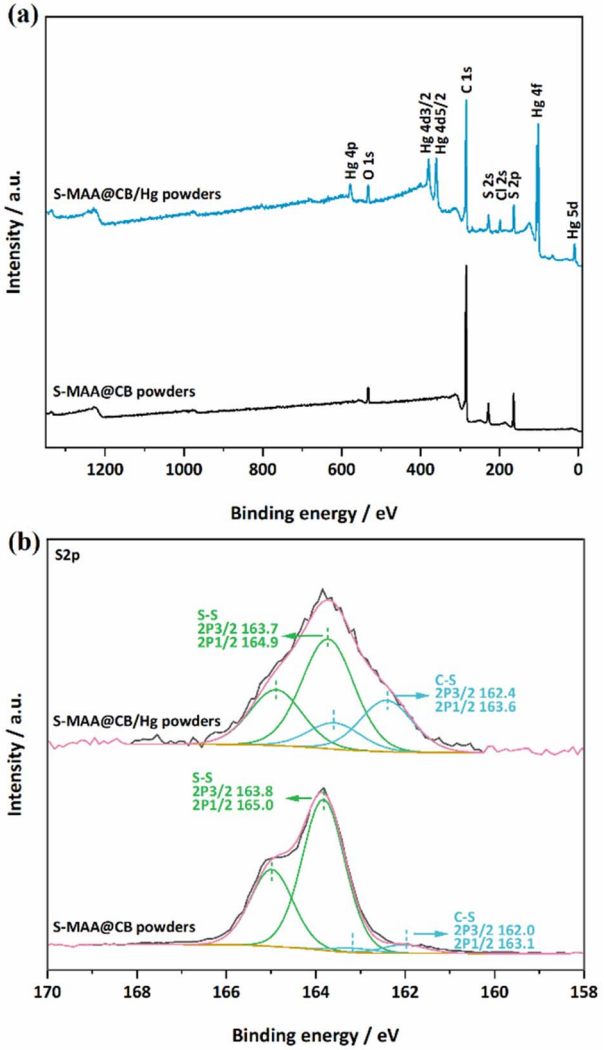

Fig. 5 (a) Full XPS and (b) S 2p spectra of S-MAA@CB and S-MAA@CB/Hg powders.

substantial change in powder size after mercury binding, indicating minimal powder aggregation. EDX maps confirms the successful sorption, with Hg detected on the complex surface (Fig. S65).

Conclusions

Hydrophilic sulfur polymers were successfully synthesized through inverse vulcanisation using various polar comonomers, with S-AA and S-NVP being reported for the first time. Structural analysis revealed that the resulting polymers comprise a mixture of linear (or crosslinked) and terminal structures. Compared to traditional hydrophobic sulfur polymers, for example polymeric sulfur–sunflower oil (water contact angle of 112.2°), these polymers reveal enhanced hydrophilicity (as low as 16.4°). The enhanced hydrophilicity enables these polymers to be wetted by water, facilitating improved interaction with aqueous mercury ions compared to traditional hydrophobic sulfur polymers. Used as coatings onto Al_2O_3 beads, sulfur polymer S-MAA exhibited superior Hg^{2+} sorption. Additional Hg^{2+} sorption assessment of S-MAA coated on SiO_2 powders, CB powders, and AC granules, showed that S-MAA@CB achieved a high Hg^{2+} uptake capacity (362 mg g^{-1}), and selectivity for Hg^{2+}. By incorporating hydrophilic comonomers, the wettability of sulfur polymers was improved. Evaluation of these polymers as coatings on diverse supporting substrates highlighted their potential utilization in industrial applications. In future studies, it is necessary to optimize inverse vulcanisation pathways under mild conditions to expand the range of suitable comonomers for hydrophilic sulfur polymers, along with developing scalable coating methods, and potential secondary crosslinking pathways post-coating to eliminate leaching.[42]

Conflicts of interest

There are no conflicts to declare.

Data availability

The data supporting this article have been included as part of the SI.

SI gives details of all synthetic materials and methods, characterisation technical details, and additional characterisation data (NMR, GC-MS, FTIR, CHNS, TGA, DSC, PXRD, TLC, solubility, photographs, gas sorption, metal uptake selectivity, XPS, SEM, and EDX). See DOI: **https://doi.org/10.1039/d5ta03218k**.

Acknowledgements

X. D. acknowledges the funding support by the China Scholarship Council (CSC) and the Materials Innovation Factory (MIF) team members for their support in operating instruments. T. H. is supported by a Royal Society University Research Fellowship.

References

1 W. J. Chung, J. J. Griebel, E. T. Kim, H. Yoon, A. G. Simmonds, H. J. Ji, P. T. Dirlam, R. S. Glass, J. J. Wie, N. A. Nguyen, B. W. Guralnick, J. Park, Á. Somogyi, P. Theato, M. E. Mackay, Y.-E. Sung, K. Char and J. Pyun, *Nat. Chem.*, 2013, **5**, 518–524.
2 F. G. Müller, L. S. Lisboa and J. M. Chalker, *Adv. Sustainable Syst.*, 2023, **7**, 2300010.
3 H. Wang, B. Zhang, R. Dop, P. Yan, A. R. Neale, L. J. Hardwick and T. Hasell, *J. Power Sources*, 2022, **545**, 231921.
4 F. Wu, S. Chen, V. Srot, Y. Huang, S. K. Sinha, P. A. van Aken, J. Maier and Y. Yu, *Adv. Mater.*, 2018, **30**, 1706643.
5 J. Pyun and R. A. Norwood, *Prog. Polym. Sci.*, 2024, **156**, 101865.
6 Y. Wuliu, W. Dong, G. Huang, H. Xie, P. Yao, J. Tan, K. Mu, Z. Zhang, Y. Chen, M. Wang, L. Tian, C. Zhu and J. Xu, *Angew. Chem., Int. Ed.*, 2024, e202419446.
7 R. A. Dop, D. R. Neill and T. Hasell, *ACS Appl. Mater. Interfaces*, 2023, **15**, 20822–20832.

8 D. Wang, Z. Tang, S. Fang, S. Wu, H. Zeng, A. Wang and B. Guo, *Carbon*, 2021, **184**, 409–417.
9 P. Yan, W. Zhao, B. Zhang, L. Jiang, S. Petcher, J. A. Smith, D. J. Parker, A. I. Cooper, J. Lei and T. Hasell, *Angew. Chem.*, 2020, **132**, 13473–13480.
10 X. Wu, J. A. Smith, S. Petcher, B. Zhang, D. J. Parker, J. M. Griffin and T. Hasell, *Nat. Commun.*, 2019, **10**, 647.
11 L. J. Dodd, Ö. Omar, X. Wu and T. Hasell, *ACS Catal.*, 2021, **11**, 4441–4455.
12 P. Yan, W. Zhao, F. McBride, D. Cai, J. Dale, V. Hanna and T. Hasell, *Nat. Commun.*, 2022, **13**, 4824.
13 J. Jia, J. Liu, Z. Q. Wang, T. Liu, P. Yan, X. Q. Gong, C. Zhao, L. Chen, C. Miao, W. Zhao, S. (Diana) Cai, X. C. Wang, A. I. Cooper, X. Wu, T. Hasell and Z. J. Quan, *Nat. Chem.*, 2022, **14**, 1249–1257.
14 J. M. M. Pople, T. P. Nicholls, L. N. Pham, W. M. Bloch, L. S. Lisboa, M. V. Perkins, C. T. Gibson, M. L. Coote, Z. Jia and J. M. Chalker, *J. Am. Chem. Soc.*, 2023, **145**, 11798–11810.
15 X. Cao, X. Liu, W. Li, D. Chen, T. Hasell, X. Wu, X. Wang and Z. Quan, *Green Chem.*, 2025, **27**, 1974–1983.
16 H. Yang, J. Huang, Y. Song, H. Yao, W. Huang, X. Xue, L. Jiang, Q. Jiang, B. Jiang and G. Zhang, *J. Am. Chem. Soc.*, 2023, **145**, 14539–14547.
17 B. Zheng, L. Zhong, X. Wang, P. Lin, Z. Yang, T. Bai, H. Shen and H. Zhang, *Nat. Commun.*, 2024, **15**, 5507.
18 J. Bao, K. P. Martin, E. Cho, K. Kang, R. S. Glass, V. Coropceanu, J. Bredas, W. O. N. Parker, J. T. Njardarson and J. Pyun, *J. Am. Chem. Soc.*, 2023, **145**, 12386–12397.
19 Y. Onose, Y. Ito, J. Kuwabara and T. Kanbara, *Polym. Chem.*, 2022, **13**, 5486–5493.
20 C. M. Marshall, J. Molineux, K. S. Kang, V. Kumirov, K. J. Kim, R. A. Norwood, J. T. Njardarson and J. Pyun, *J. Am. Chem. Soc.*, 2024, **146**, 24061–24074.
21 A. D. Tikoalu, N. A. Lundquist and J. M. Chalker, *Adv. Sustainable Syst.*, 2020, **4**, 1900111.
22 J. Yang, Q. Yang, H. Zhao and L. He, *Ind. Eng. Chem. Res.*, 2023, **62**, 3492–3502.
23 X. Deng, R. A. Dop, D. Cai, D. R. Neill and T. Hasell, *Adv. Funct. Mater.*, 2024, **34**, 2311647.
24 M. L. Eder, C. B. Call and C. L. Jenkins, *ACS Appl. Polym. Mater.*, 2022, **4**, 1110–1116.
25 L. A. Limjuco, G. M. Nisola, K. J. Parohinog, K. N. G. Valdehuesa, S. P. Lee, H. Kim and W. J. Chung, *Chem. Eng. J.*, 2019, **378**, 122216.
26 A. S. M. Ghumman, R. Shamsuddin, A. Abbasi, M. Ahmad, Y. Yoshida, A. Sami and H. Almohamadi, *Sci. Total Environ.*, 2024, **908**, 168034.
27 J. J. Dale, M. W. Smith and T. Hasell, *Adv. Funct. Mater.*, 2024, **34**, 2314567.
28 A. S. M. Ghumman, R. Shamsuddin, Z. A. Alothman, A. Waheed, A. M. Aljuwayid, R. Sabir, A. Abbasi and A. Sami, *ACS Omega*, 2024, **9**, 4831–4840.
29 C. King-Poole and H. Thérien-Aubin, *Adv. Funct. Mater.*, 2024, **34**, 2405608.
30 M. W. Thielke, L. A. Bultema, D. D. Brauer, B. Richter, M. Fischer and P. Theato, *Polymers*, 2016, **8**, 266.
31 A. P. Grimm, M. Plank, A. Stihl, C. W. Schmitt, D. Voll, F. H. Schacher, J. Lahann and P. Théato, *Angew. Chem., Int. Ed.*, 2024, **63**, e202411010.
32 S. Petcher, D. J. Parker and T. Hasell, *Environ. Sci. Water Res. Technol.*, 2019, **5**, 2142–2149.
33 S. Penczek, M. Cypryk, J. Pretula, K. Kaluzynski and P. Lewinski, *Prog. Polym. Sci.*, 2024, **152**, 101818.
34 Y. Zhang, N. G. Pavlopoulos, T. S. Kleine, M. Karayilan, R. S. Glass, K. Char and J. Pyun, *J. Polym. Sci., Part A: Polym. Chem.*, 2019, **57**, 7–12.
35 L. J. Dodd, W. Sandy, R. A. Dop, B. Zhang, A. Lunt, D. R. Neill and T. Hasell, *Polym. Chem.*, 2023, **14**, 4064–4078.
36 J. Pyun, C. F. Carrozza, S. Silvano, L. Boggioni, S. Losio, A. R. de Angelis and W. O'Neil Parker Jr, *J. Polym. Sci.*, 2022, **60**, 3471–3477.
37 J. J. Dale, J. Stanley, R. A. Dop, G. Chronowska-Bojczuk, A. J. Fielding, D. R. Neill and T. Hasell, *Eur. Polym. J.*, 2023, **195**, 112198.
38 Y. Lyu and Q. Su, *Polym. Polym. Compos.*, 2023, **31**, 1–11.
39 M. Fujita, Y. Iizuka and A. Miyake, *J. Therm. Anal. Calorim.*, 2017, **128**, 1227–1233.
40 D. I. Fortenberry and J. A. Pojman, *J. Polym. Sci., Part A: Polym. Chem.*, 2000, **38**, 1129–1135.
41 S. Guha, B. Ray and B. M. Mandal, *J. Polym. Sci., Part A: Polym. Chem.*, 2001, **39**, 3434–3442.
42 M. Mann, B. Zhang, S. J. Tonkin, C. T. Gibson, Z. Jia, T. Hasell and J. M. Chalker, *Polym. Chem.*, 2021, **13**, 1320–1327.
43 J. Magano and J. R. Dunetz, *Org. Process Res. Dev.*, 2012, **16**, 1156–1184.
44 S. Ashoka Sahadevan, X. Xiao, Y. Ma, K. Forsberg, R. T. Olsson and J. M. Gardner, *Mater. Chem. Front.*, 2023, **7**, 1374–1384.
45 N. Sagawa and T. Shikata, *Phys. Chem. Chem. Phys.*, 2014, **16**, 13262–13270.
46 S. I. Lo, P. C. Chen, C. C. Huang and H. T. Chang, *Environ. Sci. Technol.*, 2012, **46**, 2724–2730.
47 M. J. H. Worthington, M. Mann, I. Y. Muhti, A. D. Tikoalu, C. T. Gibson, Z. Jia, A. D. Miller and J. M. Chalker, *Phys. Chem. Chem. Phys.*, 2022, **24**, 12363–12373.
48 M. Algarra, M. V. Jiménez, E. Rodríguez-Castellón, A. Jiménez-López and J. Jiménez-Jiménez, *Chemosphere*, 2005, **59**, 779–786.
49 X. Liu, Y. Lu, Q. Zeng, P. Chen, Z. Li, X. Wen, W. Wen, Z. Li and L. Zhang, *ChemSusChem*, 2020, **13**, 715–723.
50 H. Wang and J. J. Zhu, *Ultrason. Sonochem.*, 2004, **11**, 293–300.